https://ntrs.nasa.gov/search.jsp?R=19760018846 2020-03-22T14:14:33+00:00Z

General Disclaimer

One or more of the Following Statements may affect this Document

- This document has been reproduced from the best copy furnished by the organizational source. It is being released in the interest of making available as much information as possible.
- This document may contain data, which exceeds the sheet parameters. It was furnished in this condition by the organizational source and is the best copy available.
- This document may contain tone-on-tone or color graphs, charts and/or pictures, which have been reproduced in black and white.
- This document is paginated as submitted by the original source.
- Portions of this document are not fully legible due to the historical nature of some of the material. However, it is the best reproduction available from the original submission.

Produced by the NASA Center for Aerospace Information (CASI)

MS-MSFC-1981

MS-MSFC-1981

Final Report

(NASA-CR-144330) RESULTS OF AN ANALYTICAL STUDY OF SPACECRAFT DEPOSITION CONTAMINATION BY INTERNAL REFLECTION SPECTROSCOPY FINAL REPORT (TELEDYNE BROWN ENGINEERING) 33 P HC $4.00 CSCL 20F G3/74
N76-25934
UNCLAS
42218

RESULTS OF AN ANALYTICAL STUDY OF SPACECRAFT DEPOSITION CONTAMINATION BY INTERNAL REFLECTION SPECTROSCOPY

March 31, 1976

Cummings Research Park • Huntsville, Alabama 35807

ABSTRACT

Outgassing, deposition, and desorption kinetics of RTV-602 and RTV-560 silicone compounds are studied as examples of optical surface contaminants and their behavior in a space environment. The use of internal reflection spectroscopy (IRS) is shown to provide a viable means of real-time, in-situ identification of contaminant characteristics. The instrumental techniques are proposed as the basis of further investigations and the development of flight hardware.

Approved

N. E. Chatterton, Ph.D
Manager, Research

Submitted by

Tripty Mookherji, Ph.D
Principal Investigator

W. A. Grenard
Manager, Systems Analysis Department

TABLE OF CONTENTS

		Page
1.	INTRODUCTION	1-1
2.	PRINCIPLES OF INTERNAL REFLECTION SPECTROSCOPY	2-1
3.	RESULTS AND DICUSSION	3-1
	3.1 Absorption Spectra	3-1
	3.2 Vacuum and Thermal Desorption Kinetics	3-11
	3.3 Ultraviolet Radiation Effects	3-12
	3.4 In-Situ Deposition Study	3-14
4.	CONCLUSIONS AND RECOMMENDATION	4-1
5.	REFERENCES	5-1

LIST OF ILLUSTRATIONS

Figure	Title	Page
2-1	Internal Reflectivity of an Interface as a function of Angle of Incidence at $\lambda = 0.4$ μm for $\eta_{21} = 0.333$ and Various Values of Absorption Coefficient	2-4
2-2	Standing-Wave Amplitudes Established near a Totally Reflecting Interface (Ref. 5)	2-7
2-3	Reflection at Interface of Media	2-10
3-1	Absorption Spectrum of RTV-560	3-2
3-2	Absorption Spectrum of RTV-602	3-3
3-3	Vacuum Desorption of RTV-602	3-4
3-4	Thermal Desorption of RTV-602	3-5
3-5	Vacuum Desorption of RTV-560	3-6
3-6	Thermal Desorption of RTV-560	3-7
3-7	Semilog Plot of Normalized Absorption as a Function of Temperature, RTV-602	3-8
3-8	Semilog Plot of Normalized Absorption as a Function of Temperature, RTV-560	3-9
3-9	Vacuum Deposition of RTV-602	3-10

1. INTRODUCTION

Problems imposed by outgassing and subsequent film condensation of materials of unknown composition and origin have been observed on space vehicle windows during a number of Gemini and Apollo flights. These deposits have interfered with vision and photography. For Skylab, the column density resulting from venting of water and outgassing products is found to be on the order of 10^4 and 10^{11}, respectively. The scattering due to the contaminant cloud was rather high, and bright dust particles produced streaks on SO-52 films. The rendezvous window in the Skylab-4 mission was found to be badly contaminated. Such contaminants on critical optical surfaces, thermal control coatings, solar cells, and other experimental equipment of the Shuttle and other space systems could adversely affect the very basis of the space program.

A recent study of the outgassed products from Shuttle thermal protection system (TPS) panels showed the presence of silicone along with other chemicals (Ref. 1). The TPS was found to contaminate the vacuum chamber very badly in the environment of hard vacuum and ultraviolet irradiation.

Plans are now under way to use reaction control system (RCS) engines in Shuttle. Both mono- and bi-propellant RCS engine plumes contain contaminants. Bi-propellant systems give rise to more contaminants, consisting of water, monomethylhydrazine hydrate, etc. These can affect the optical surfaces very adversely through chemical reaction, abrasion, and deposition of absorbing and reflecting material.

Furthermore, photons in the ultraviolet region and solar protons and electrons possess sufficient energy to cause fission of chemical bonds of the contaminants. The resulting free radicals may react in a wide variety of ways, resulting in polymerization and cross-linking of a very complex nature and ultimately in the formation of a hard carbonaceous glaze of indeterminant stoichiometry. The effect of ultraviolet irradiation on some representative contaminant materials has already been studied

(Refs. 2, 3). To locate and control the sources of contamination and to devise the appropriate cleaning technique, it is first necessary to identify the substances absorbed on the surfaces and to correlate these contaminants with substances detected in the cabin atmosphere.

The present study is concerned with the identification of the infrared spectra of RTV-602 and RTV-560, in-situ monitoring of the vacuum and thermal desorption kinetics of these silicones, and ultraviolet irradiation effects on these silicones. During the process of this study, the use of internal reflection spectroscopy as a tool for identification and monitoring of contaminating materials was further developed and applied to in-situ measurements. The results of the preliminary investigations demonstrate the significant potential of the technique to provide real-time information on contaminants of orbiting spacecraft systems.

2. PRINCIPLES OF INTERNAL REFLECTION SPECTROSCOPY

The optical properties of absorbing media may be described quantitatively by the complex refractive index, $\tilde{N} = n + ik$, where n, the real part of the refractive index, is defined as the ratio of the velocity of light in vacuum, c, to the phase velocity, v, in the dielectric, of a plane electromagnetic wave having constant amplitude along a wavefront (Ref. 4),

$$n = c/v. \tag{2-1}$$

The imaginary part of the complex refractive index, k, often called the extinction coefficient, describes the damping of the wave as it traverses the absorbing medium, and is defined by the relation

$$E = E_o \exp\left(-\frac{2\pi kz}{\lambda}\right) \tag{2-2}$$

where

- z - coordinate in the direction of propagation
- E_o - amplitude of the electromagnetic wave at $z = 0$
- E - amplitude at z
- λ - wavelength of the electromagnetic wave in vacuum.

The theory of reflection and transmission of light by thin films has been discussed in many texts. Expressions for the reflectance, R, at a given wavelength are obtained by the application of boundary conditions to Maxwell's equations for a plane electromagnetic wave incident on the boundary between two media.

When a plane wave falls onto a boundary between two homogeneous media of different optical properties, it is split into two waves: a transmitted wave proceeding into the second medium and a reflected wave propagated back into the first medium. The existence of these two waves can be demonstrated from the boundary conditions, since it is easily seen

that these conditions cannot be satisfied without postulating both the transmitted and the reflected wave. The transmitted beam is refracted according to Snell's law:

$$n_1 \sin \theta = n_2 \sin \phi \tag{2-3}$$

where

n_1 - the refractive index in medium 1

n_2 - the refractive index in medium 2

θ - the angle of incidence in medium 1

ϕ - the angle of refraction in medium 2.

For the reflected beam, the angle of reflection is equal to the angle of incidence. The reflected amplitudes for unit incident amplitudes for light with the electric field vector perpendicular and parallel to the plane of incidence, respectively, are given by Fresnel's equations,

$$R_{\perp} = \frac{n_1 \cos \theta - n_2 \cos \phi}{n_1 \cos \theta + n_2 \cos \phi} \tag{2-4}$$

$$R_{\parallel} = \frac{n_2 \cos \theta - n_1 \cos \phi}{n_2 \cos \theta + n_1 \cos \phi} . \tag{2-5}$$

For internal reflection, i.e., when the light approaches the interface from the denser medium, both $R_{\perp}$ and $R_{\parallel}$ become 100 percent at the critical angle, θ_c, given by

$$\theta_c = \sin^{-1} \left(\frac{n_2}{n_1}\right) = \sin^{-1} n_{21} \tag{2-6}$$

where $n_{21} \equiv n_2/n_1$.

For angles of incidence larger than θ_c, ϕ becomes imaginary. In this case, the refracted angle, ϕ, may be obtained from the relation

$$\cos \phi = \left(1 - \sin^2 \phi\right)^{1/2}$$

or

$$\cos \phi = i \; \frac{(\sin^2 \theta - n_{21}{}^2)^{1/2}}{n_{21}} . \tag{2-7}$$

Substituting Equation 2-7 into Equations 2-4 and 2-5, the Fresnel reflection equations become

$$R_{\perp} = \frac{\cos\,\theta - i\,(\sin^2\,\theta - n_{21}{}^2)^{1/2}}{\cos\,\theta + i\,(\sin^2\,\theta - n_{21}{}^2)^{1/2}} \tag{2-8}$$

and

$$R_{\parallel} = \frac{n_{21}{}^2\,\cos\theta - i\,(\sin^2\,\theta - n_{21}{}^2)^{1/2}}{n_{21}{}^2\,\cos\theta + i\,(\sin^2\,\theta - n_{21}{}^2)^{1/4}}\;. \tag{2-9}$$

Then, when n_{21} is real (i.e., when the media are transparent, or non-absorbing), the reflection is total for angles of incidence between θ_c and 90 degrees.

If the rarer medium is absorbing, the reflectivity can be calculated by substituting in Equations 2-8 and 2-9 the complex refractive index for n_2, i.e.,

$$\tilde{N}_2 = n_2 + i\,k_2. \tag{2-10}$$

The absorption coefficient, α, is related to the extinction coefficient, k, by

$$k = \frac{\alpha\lambda}{4\pi} \tag{2-11}$$

where λ is the wavelength at which k is determined.

The Fresnel equations become complicated upon substitution of the complex refractive index, and the use of a computer is necessary for solution of the equations.

The rarer absorbing medium strongly affects the reflectivity for internal reflection, particularly in the vicinity of the critical angle. The critical angle is no longer as sharp as it is with a nonabsorbing medium; the reflectivity curves become less steep in this region, as shown in Figure 2-1. The absorption loss is quite large near the critical angle, is greater for parallel polarization than it is for perpendicular polarization, and decreases with increasing angle of incidence for both polarizations.

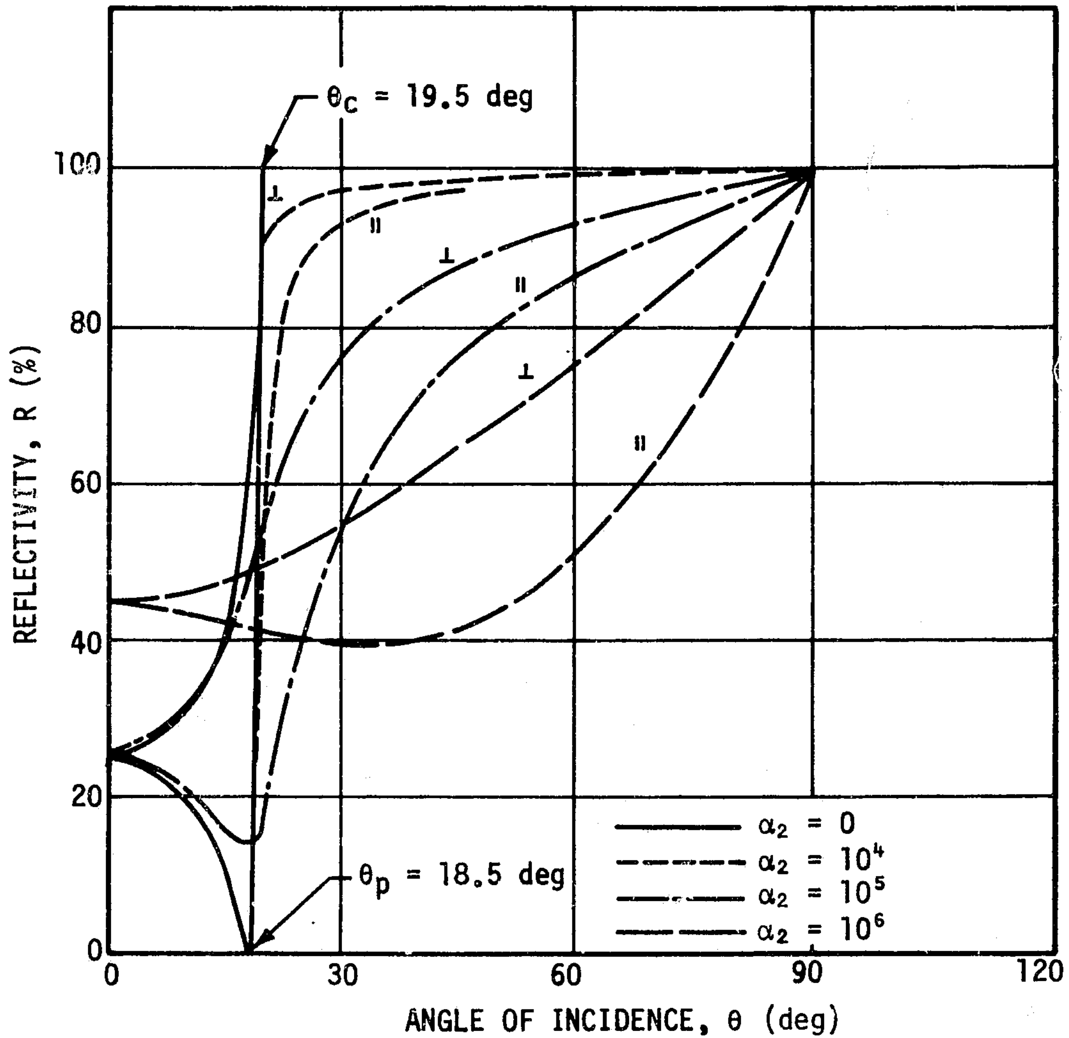

FIGURE 2-1. INTERNAL REFLECTIVITY OF AN INTERFACE AS A FUNCTION OF ANGLE OF INCIDENCE AT $\lambda = 0.4$ μm FOR $\eta_{21} = 0.333$ AND VARIOUS VALUES OF ABSORPTION COEFFICIENT

REPRODUCIBILITY OF THE ORIGINAL PAGE IS POOR

This behavior is the basis for attenuated total reflectance (ATR) spectroscopy, since the internal reflection, particularly in the vicinity of the critical angle, may be extremely sensitive to changes in the absorption coefficient.

In ATR, the reflection loss is the parameter measured. It is convenient to define an absorption parameter, a, as the reflection loss per reflection; i.e., for a single reflection (Ref. 5),

$$R = 1 - a \; . \tag{2-12}$$

It is useful to set up the equations for ATR in such a manner as to be directly comparable to transmission spectroscopy. For a material of actual thickness, d, and with an absorption coefficient, α, the transmittance, T, is given by

$$T = \exp(-\alpha d) \; . \tag{2-13}$$

For $\alpha d << 1$,

$$T \approx 1 - \alpha d \; . \tag{2-14}$$

Equations 2-14 and 2-12 are of the same form. It is convenient to define an "effective thickness", d_e, such that

$$R \equiv 1 - \alpha d_e \tag{2-15}$$

where

α - true absorption coefficient

d_e - parameter, dependent on the optical properties of the media involved and the angle of incidence and polarization of the radiation incident on the media interface, which gives the correct R for the specified conditions.

Thus, for N internal reflections

$$R^N = (1 - \alpha d_e)^N \; .$$

Equations 2-14 and 2-15 are useful for comparing the measured quantities R and T for known film thickness and effective thickness. However, if $\alpha d \geqq 1$, it is necessary to compare R and T obtained from Equation 2-14. To relate the effective thickness to the actual film thickness, it is

necessary to consider the establishment of standing waves at the reflecting interface.

It can be shown from Maxwell's equations that standing waves are established normal to a totally reflecting surface because of the superposition of the incoming and reflected waves (Ref. 4). For total internal reflection, there is a sinusoidal variation of the electric field amplitude with distance from the surface in the denser medium. By selecting the proper angle of incidence, it is possible to locate the antinode (the electric field maximum) at the surface and thus obtain the most efficient energy transfer across the interface. An evanescent wave exists in the rarer medium whose electric field amplitude decays exponentially with distance from the surface (Figure 2-2). Consequently, one can define a depth of penetration, d_p, as the distance required for the electric field, E, to fall to 1/e of its d_p value at the surface, E_o, i.e.,

$$E = E_o \exp(-z/d_p) \quad . \tag{2-16}$$

The depth of penetration is given by

$$d_p = \frac{\lambda_1}{2\pi} (\sin^2 \theta - n_{21}{}^2)^{-\frac{1}{2}} \tag{2-17}$$

where $\lambda_1 = \lambda/n_1$ is the wavelength in the denser medium and θ is the angle on incidence at the interface.

Assuming low absorption (i.e., $\alpha d < 0.1$), the effective thickness is calculated from the electric fields for zero absorption and is (Ref. 5)

$$d_e = \frac{n_{21}}{\cos \theta} \int_0^d E^2 (z)\, dz \tag{2-18}$$

where z is the distance in the rarer medium and d is the thickness of the medium, and E(z) is the electric field amplitude of the incident radiation within the sample. Substituting for E and solving, one obtains

$$d_e = \frac{n_{21}}{\cos \theta} \frac{E_o{}^2 d_p}{2} [1 - \exp(-2d/d_p)] \quad . \tag{2-19}$$

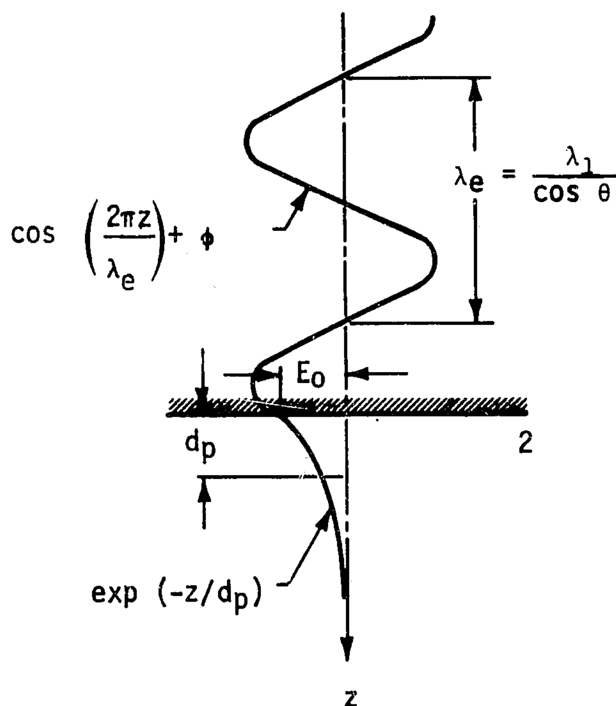

FIGURE 2-2. STANDING-WAVE AMPLITUDES ESTABLISHED NEAR A TOTALLY REFLECTING INTERFACE (Ref. 5)

When $d \ll d_p$, d_e is given by

$$d_e = \frac{n_{21} E_o^2 d}{\cos \theta} \tag{2-20}$$

while for $d \gg d_p$, d_e is given by

$$d_e = \frac{n_{21} E_o^2 d_p}{2 \cos \theta} . \tag{2-21}$$

These equations indicate that four factors influence the strength of coupling of the evanescent wave with the absorbing medium. These four factors are the depth of penetration, d_p, the electric field strength at the interface, E_o, the sampling area, and the refractive index matching.

The great advantage of ATR spectroscopy is that because of a reflectance of 1 for nonabsorbing media, many reflections can be utilized without reflection losses. Hence, small absorption losses for weakly

REPRODUCIBILITY OF THE ORIGINAL PAGE IS POOR

absorbing films can be multiplied many times without a simultaneous increase in "noise" due to substrate reflection inefficiencies.

As mentioned before for N reflections, the measured reflectivity is

$$R^N = (1 - \alpha d_e)^N . \tag{2-22}$$

For $\alpha d_e < 0.1$,

$$R^N \approx 1 - N\alpha d_e . \tag{2-23}$$

Then to maximize the absorption contrast, the product Nd_e should be maximized. Since d_e depends on the polarization of the incident radiation, it is convenient to consider the components perpendicular and parallel to the angle of incidence separately. Harrick (Ref. 6) has calculated the electric field amplitudes near a totally reflecting, nonabsorbing interface. The equations for a maximum amplitude of unity are:

$$E_{yo} = \frac{2 \cos \theta}{(1 - n_{21}{}^2)^{\frac{1}{2}}} \tag{2-24}$$

$$E_{xo} = E_{yo} \frac{(\sin^2 \theta - n_{21}{}^2)^{\frac{1}{2}}}{\left[(1 + n_{21}{}^2) \sin^2 \theta - n_{21}{}^2\right]^{\frac{1}{2}}} \tag{2-25}$$

and

$$E_{zo} = E_{yo} \frac{\sin \theta}{\left[(1 + n_{21}{}^2) \sin^2 \theta - n_{21}{}^2\right]^{\frac{1}{2}}} . \tag{2-26}$$

The perpendicular and parallel components are given by

$$E_{\perp} = E_{yo} \tag{2-27}$$

$$E_{\parallel} = (|E_{xo}|^2 + |E_{zo}|^2)^{\frac{1}{2}} . \tag{2-28}$$

Substituting Equations 2-27 and 2-28 for E_o in Equation 2-19, one obtains

$$d_{e\perp} = \frac{4 n_{21} \cos \theta}{(1 - n_{21}{}^2)} \frac{d_p}{2} [1 - \exp (-2d/d_p)] . \tag{2-29}$$

and

$$d_{e\parallel} = d_{e\perp} \frac{(2 \sin^2 \theta - n_{21}{}^2)}{[(1 + n_{21}{}^2) \sin \theta \ - n_{21}{}^2]} \quad . \tag{2-30}$$

Note that since d_p is wavelength-dependent (Equation 2-17), both d_e and d_e will increase with wavelength when d is not small relative to the wavelength of the incident radiation.

For most practical multiple reflection cell designs that retain the initial polarization, the number of reflections, N, is proportional to cot θ, so that

$$Nd_{e\perp} \propto d_{e\perp} \cot \theta \tag{2-31}$$

and

$$Nd_{e\parallel} \propto d_{e\parallel} \cot \theta \ . \tag{2-32}$$

To maximize the observed change in reflectance, one should maximize Equation 2-31 when using perpendicularly polarized radiation and Equation 2-32 when using parallel polarized radiation.

Equations 2-29 and 2-30 are general within the low absorption approximation. However, it must be pointed out that when medium 2 is very thin, the electric field amplitudes are determined by media 1 and 3 (Figure 2-3) and for this condition,

$$E_{\perp} = \frac{2 \cos \theta}{(1 - n_{31}{}^2)^{1/2}} \ . \tag{2-33}$$

$$E_{\parallel} = E \ \frac{[(1 + n_{31}{}^4) \sin^2 \theta - n_{31}{}^2]^{1/2}}{[(1 + n_{31}{}^2) \sin^2 \theta - n_{31}{}^2]^{1/2}} \tag{2-34}$$

so that

$$Nd_{e\perp} \propto \frac{4 \ n_{21} \cos \theta \cot \theta}{(1 - n_{31}{}^2)} \ \frac{d_p}{2} \ [1 - \exp(-2d/d_p)] \tag{2-35}$$

and

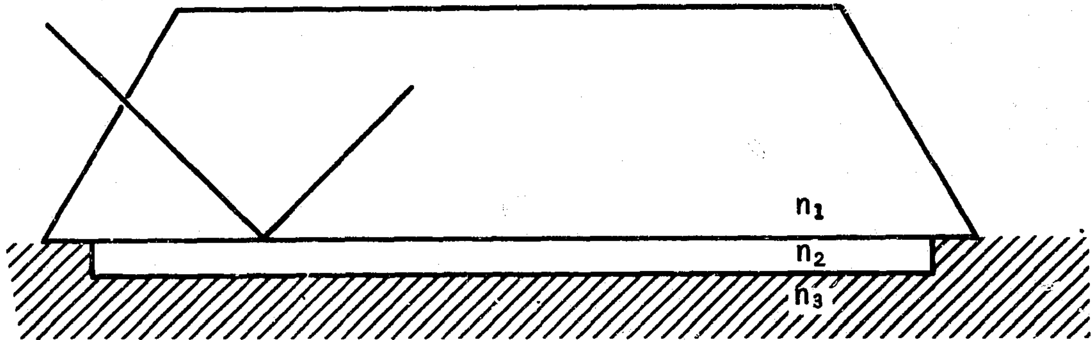

FIGURE 2-3. REFLECTION AT INTERFACE OF MEDIA

$$Nd_{e||} \propto Nd_{e\perp} \frac{[(1 + n_{31}{}^2) \sin^2 \theta - n_{31}{}^2]}{[(1 + n_{31}{}^2) \sin^2 \theta - n_{31}{}^2]} \; . \qquad (2\text{-}36)$$

For a given sample material, n_2 is fixed. Then to obtain maximum sensitivity, one must select the combination of θ, n_2, and n_1 which will optimize Equation 2-31 or Equation 2-35 when working with perpendicularly polarized light or Equation 2-32 or Equation 2-36 when working with parallel polarized light.

REPRODUCIBILITY OF THE
ORIGINAL PAGE IS POOR

3. RESULTS AND DISCUSSION

The results gathered during the present study are presented in Figures 3-1 through 3-9. Experimental procedures and apparatus were the same as before (Refs. 1, 2).

Materials were deposited on the crystal ATR by two techniques: condensation of thermally outgassed products under ambient atmosphere and condensation of thermally outgassed products from cured materials under vacuum.

These results are discussed in terms of identification of the absorption band, vacuum and thermal desorption kinetics, and effects of ultraviolet irradiation.

3.1 ABSORPTION SPECTRA

Figure 3-1 shows the absorption spectrum of RTV-560 before and after ultraviolet radiation. The characteristic siloxane band is between 9.0 and 10.0 micrometers. The double-peak characteristic of this band at 9.25 and 9.75 micrometers, instead of a single-peak somewhere between 9.0 and 10.0 micrometers, shows the polymeric characteristic. The methyl group that is attached to the silicon has its characteristic absorption at 7.95, 12.0, and 12.5 micrometers. The methyl group has its stretching and deformation absorptions at 3.35 and 7.25 micrometers. The absorption bands due to the phenyl group attached to the silicon are located at 7.0 and 13.5 micrometers.

Figure 3-2 shows the infrared absorption spectrum of RTV-602. The characteristic absorption band of long-chain siloxane is located between 9.0 and 10.0 micrometers, with two peaks at 9.25 and 9.75 micrometers. Methyl groups attached to silicon have characteristic absorptions at 7.95 and 12.5 micrometers. The absorption bands at 11.5 and 12.5 micrometers indicate that two methyl groups are attached to the silicon. Methyl stretching and deformation absorptions are at 3.35 and 7.25 micrometers.

REPRODUCIBILITY OF THE
ORIGINAL PAGE IS POOR

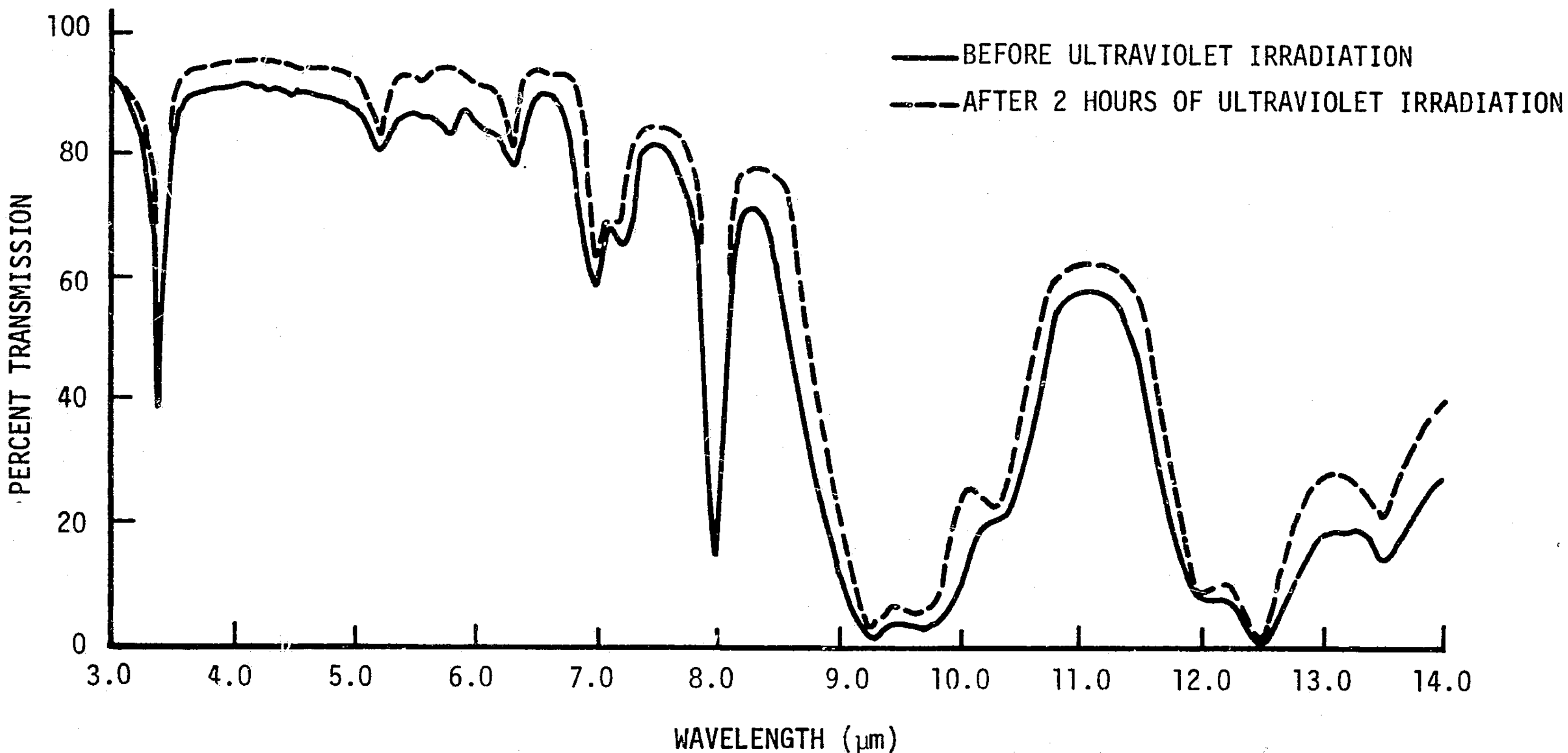

FIGURE 3-1. ABSORPTION SPECTRUM OF RTV-560

REPRODUCIBILITY OF THE
ORIGINAL PAGE IS POOR

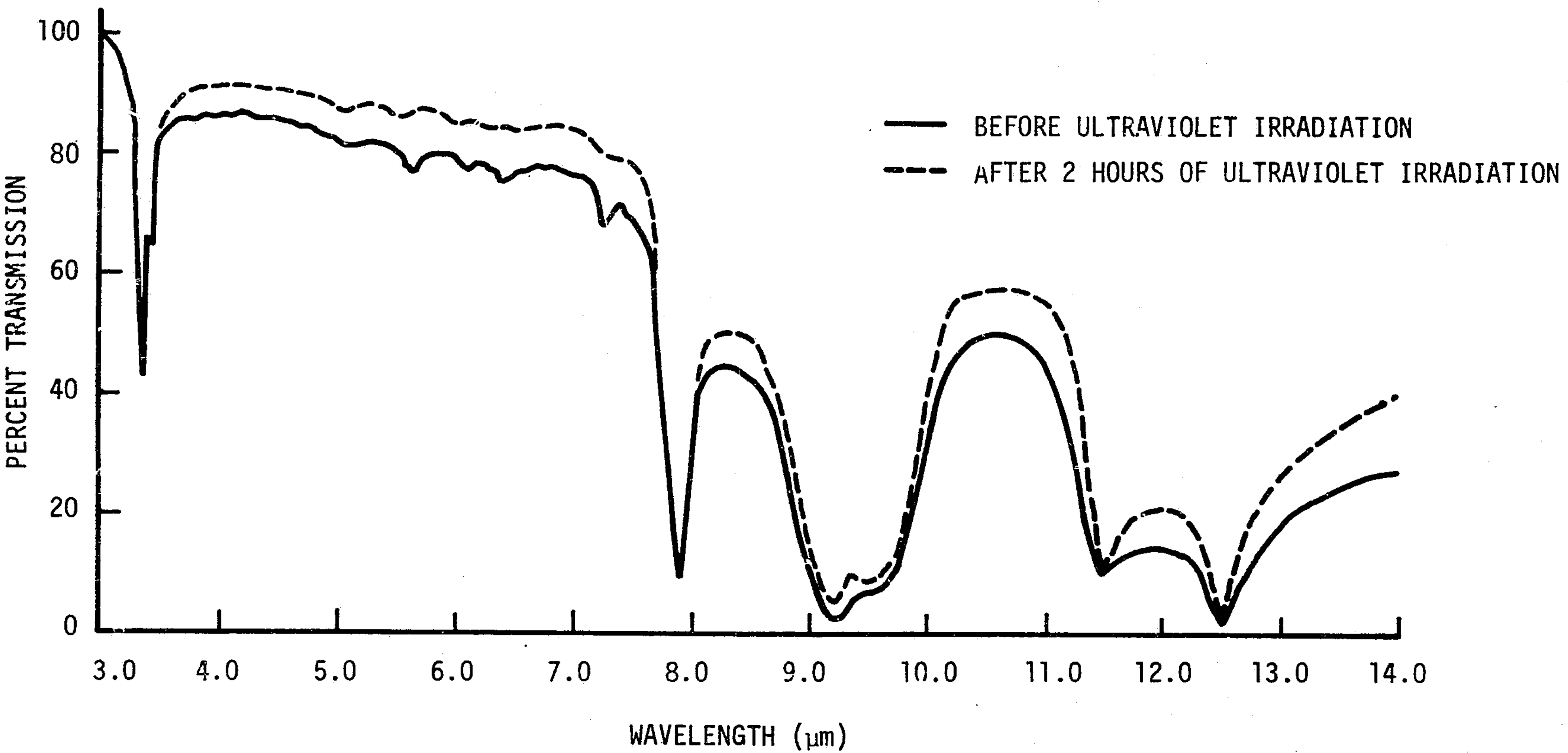

FIGURE 3-2. ABSORPTION SPECTRUM OF RTV-602

REPRODUCIBILITY OF THE
ORIGINAL PAGE IS POOR

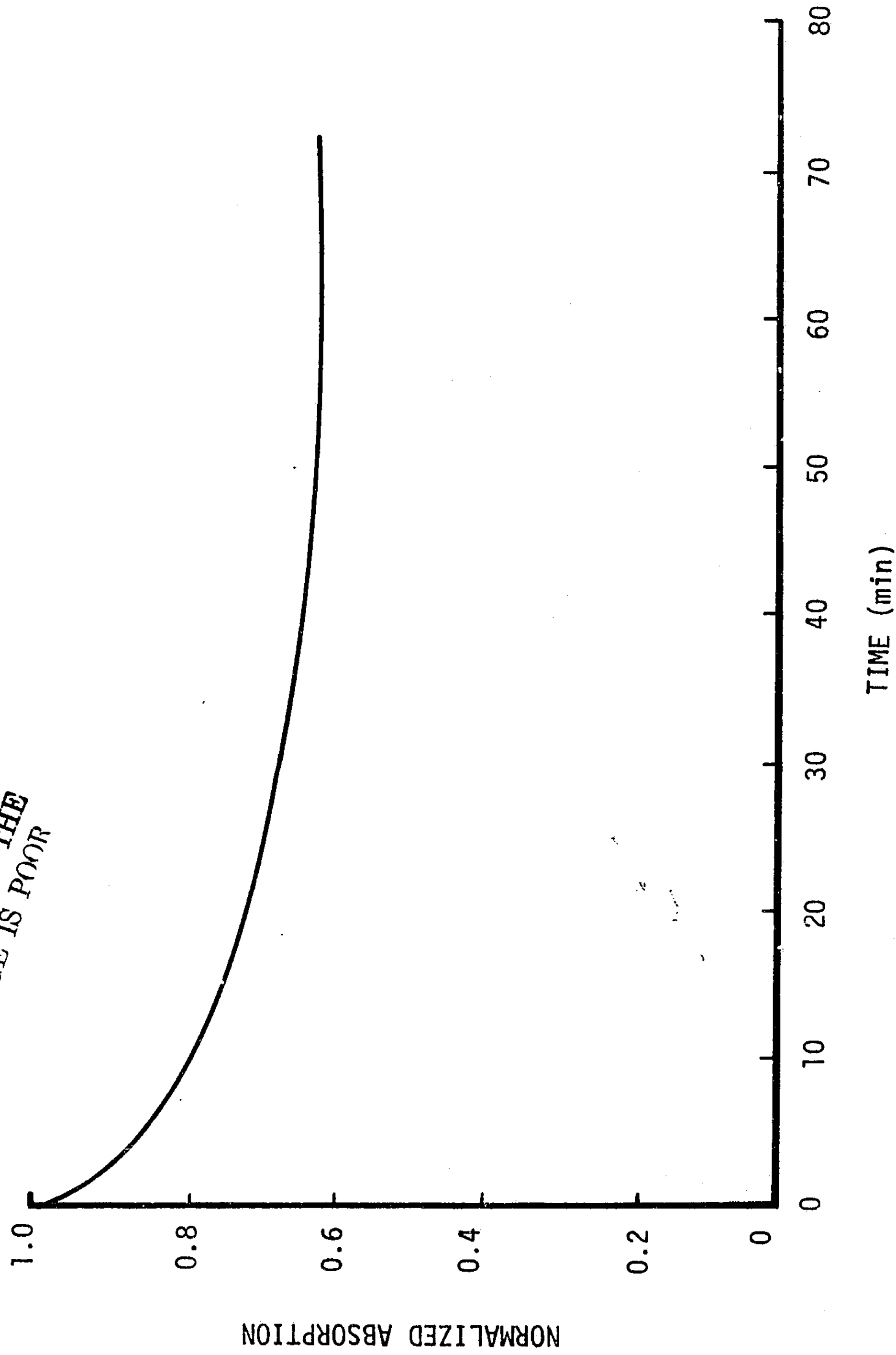

FIGURE 3-3. VACUUM DESORPTION OF RTV-602

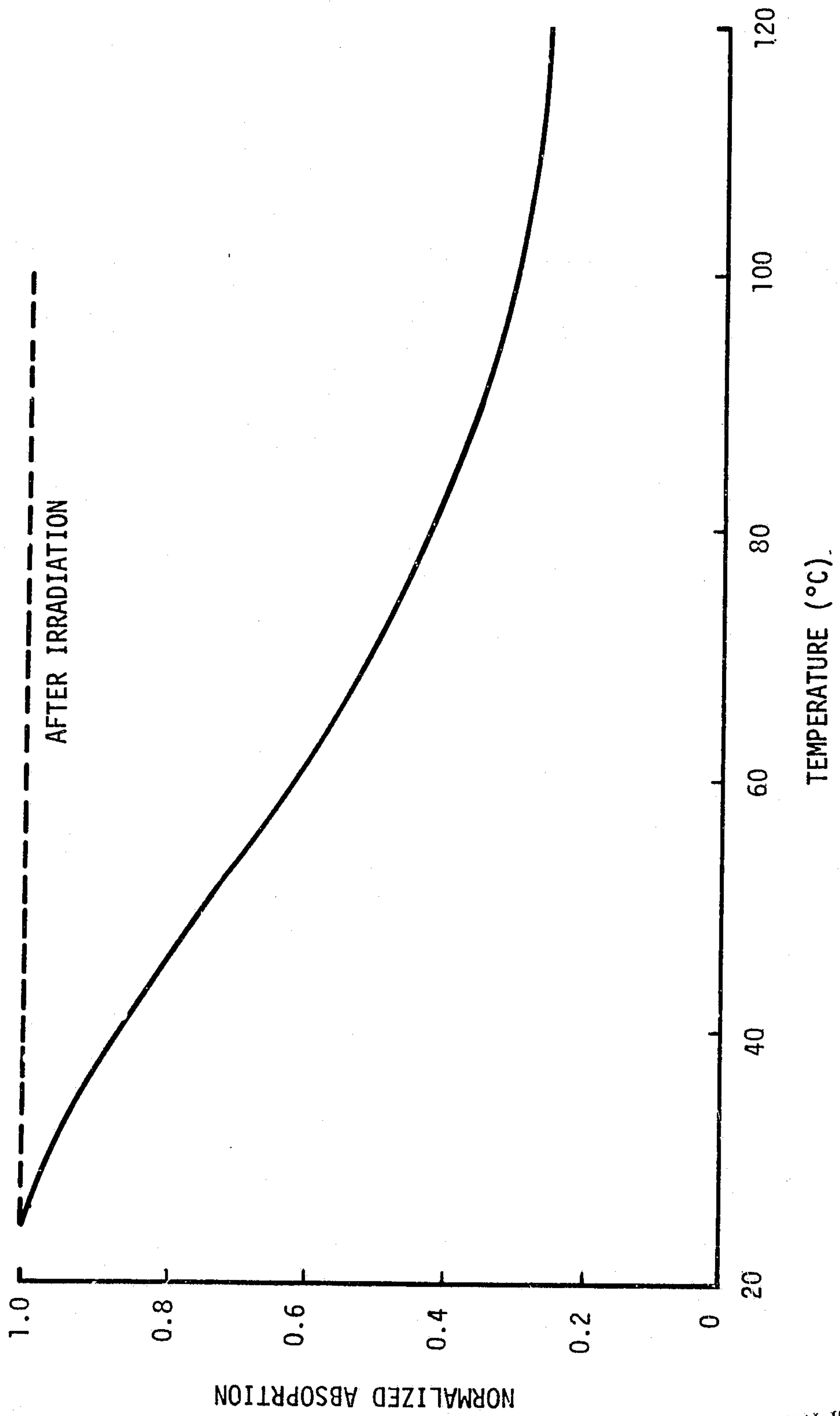

FIGURE 3-4. THERMAL DESORPTION OF RTV-602

REPRODUCIBILITY OF THE
ORIGINAL PAGE IS POOR

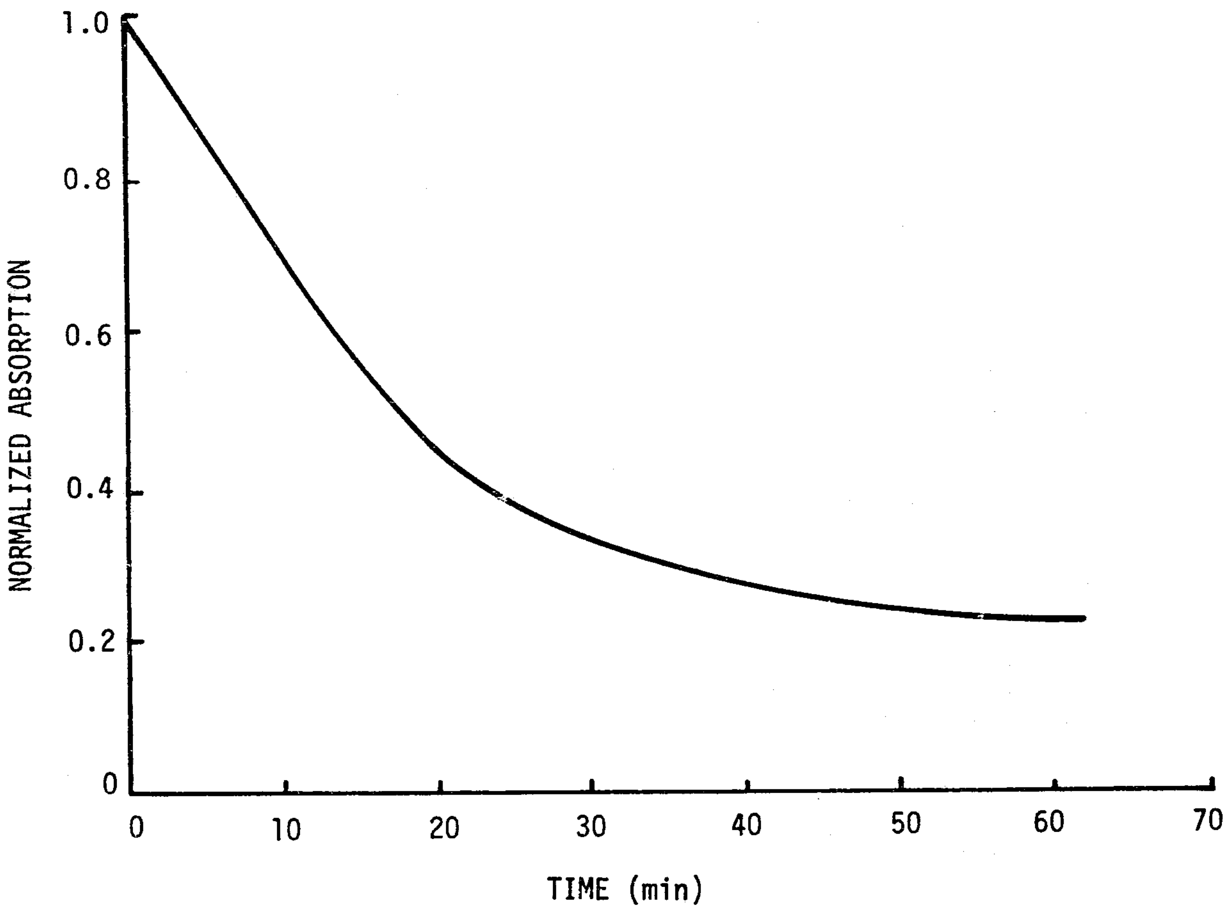

FIGURE 3-5. VACUUM DESORPTION OF RTV-560

REPRODUCIBILITY OF THE ORIGINAL PAGE IS POOR

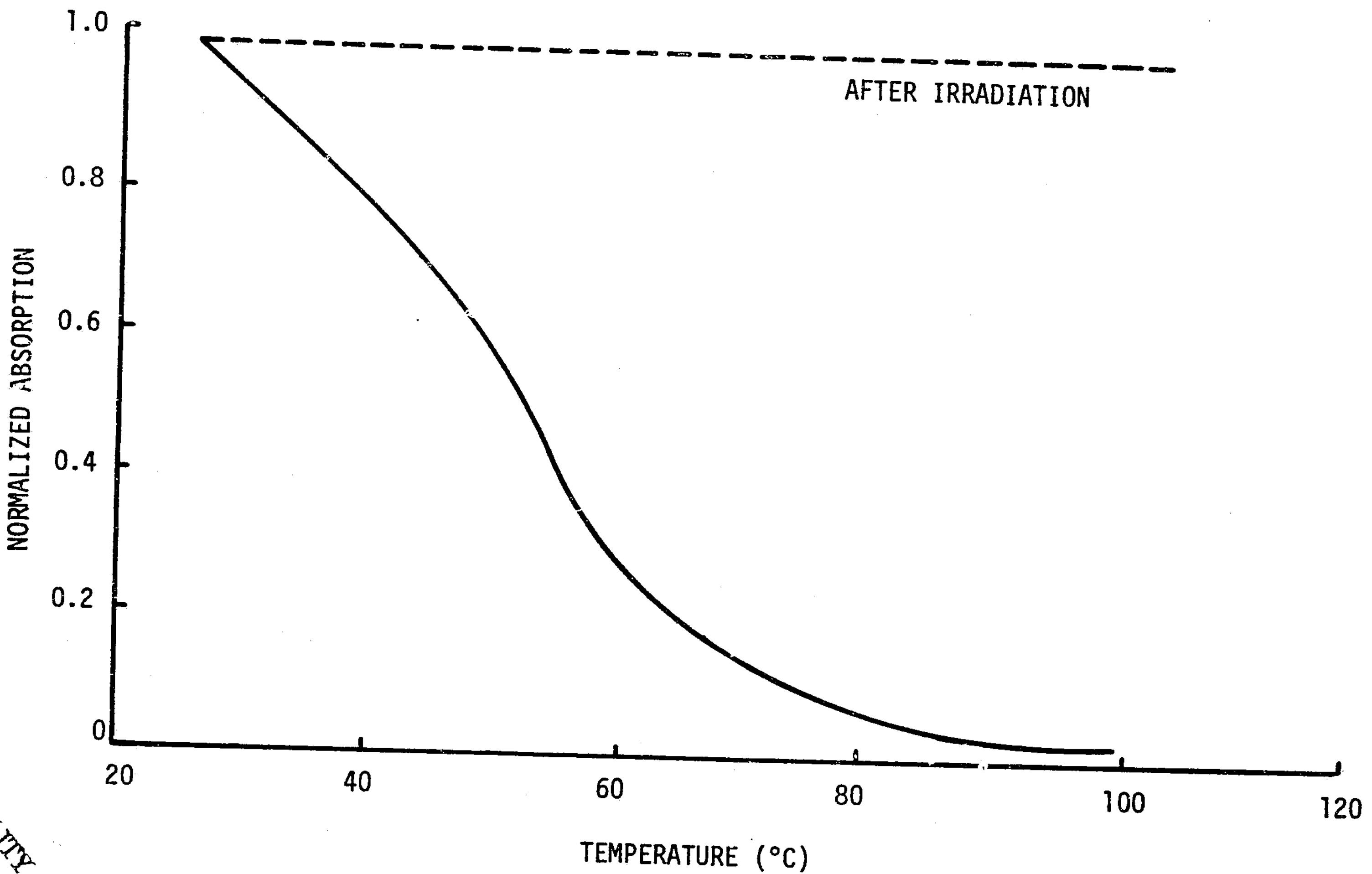

FIGURE 3-6. THERMAL DESORPTION OF RTV-560

REPRODUCIBILITY OF THE ORIGINAL PAGE IS POOR

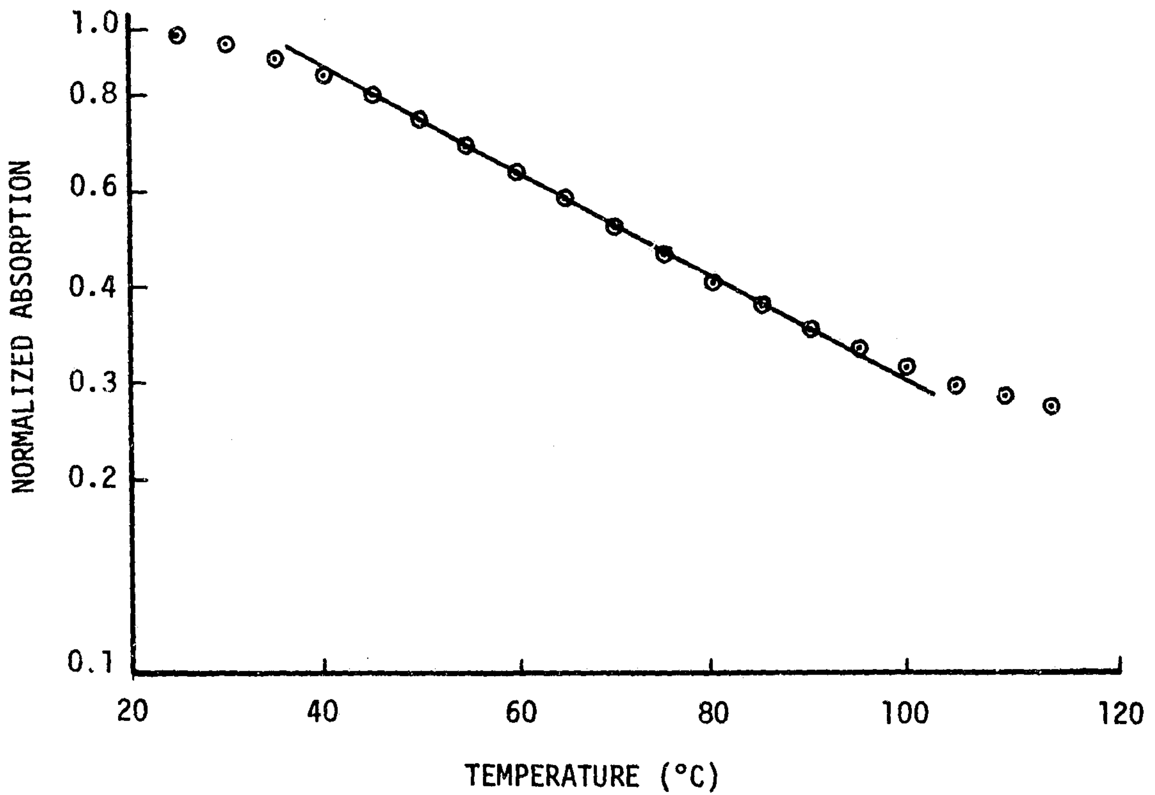

FIGURE 3-7. SEMILOG PLOT OF NORMALIZED ABSORPTION AS A FUNCTION OF TEMPERATURE, RTV-602

ORIGINAL PAGE IS POOR

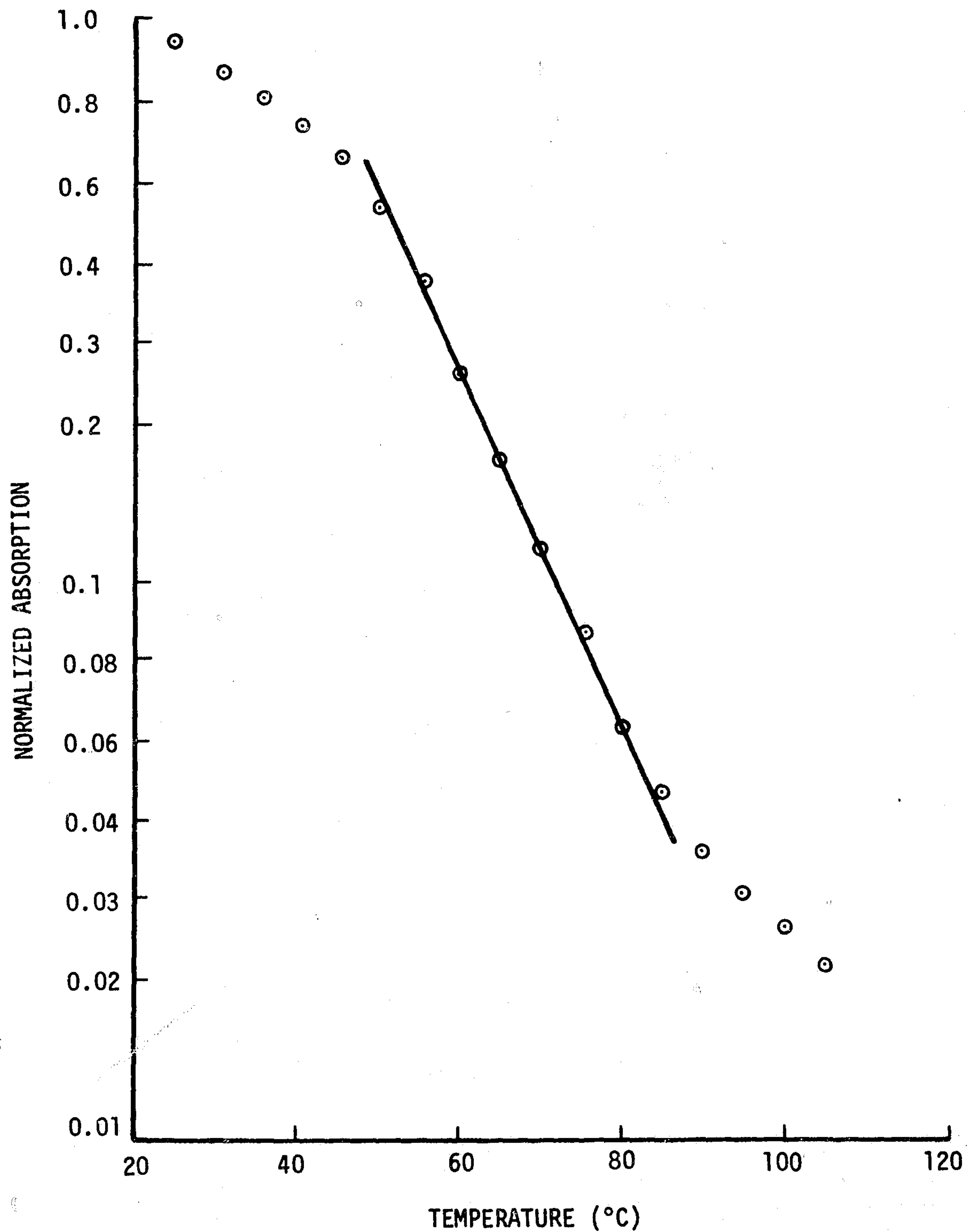

FIGURE 3-8. SEMILOG PLOT OF NORMALIZED ABSORPTION AS A FUNCTION OF TEMPERATURE, RTV-560

ODUCIBILITY
INAL PAGE IS

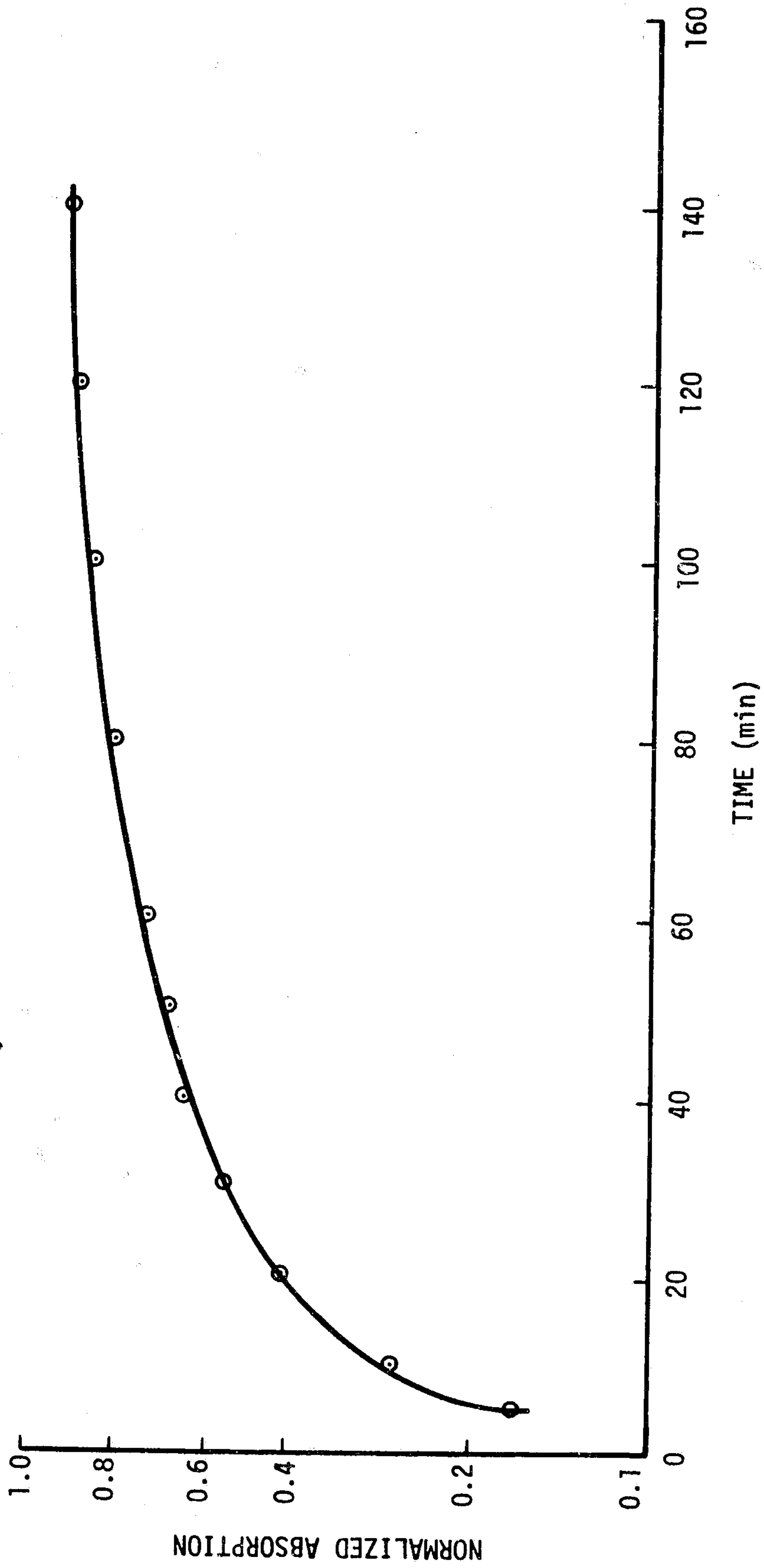

REPRODUCIBILITY OF THE ORIGINAL PAGE IS POOR

FIGURE 3-9. VACUUM DEPOSITION OF RTV-602

The two spectra are similar, except for the phenyl absorption band, since both have a methyl silicone base.

3.2 VACUUM AND THERMAL DESORPTION KINETICS

Vacuum and thermal desorption kinetics of RTV-602 are shown in Figures 3-3 and 3-4, respectively. Vacuum desorption is very small and goes to zero in about 50 minutes. The desorption appears to follow an exponential low in the time range of 15 to 45 minutes. As can be seen, only about 40 percent of the deposited material desorbs under vacuum.

Thermal desorption studies were started when vacuum desorption was no longer noticeable. The nature of thermal desorption appears to depend on the deposited film thickness. For very thick films, the thermal desorption appears to be linear. As the thickness of the film decreases, the desorption kinetics become exponential in nature. This is shown in Figure 3-7. The exponential decay in the temperature range of 40°C and 95°C can be expressed by

$$D_T = D_o e^{-\alpha T}$$

where

D_T - desorption at any temperature, T

D_o - pre-exponential factor

α - activation energy of desorption.

The activation energy of desorption calculated using the above equation turns out to be $0.019°C^{-1}$. It can be seen that all the material deposited onto KRS-5 does not desorb, and about 25 percent of the material is still left at about 120°C. Heating the ATR crystal up to 160°C did not produce further noticeable desorption. It is possible that the desorption is exponential with different activation energies for different ranges of temperature. This could not be verified in the temperature range of study; the few data points between 20 to 40°C and 100 to 120°C do not allow it. If measurements could be started at much lower temperature then some definite conclusion could be made.

The results of the desorption kinetics tests of RTV-560 are shown in Figures 3-5 and 3-6. This material desorbs much more than RTV-602 under vacuum and appears to follow an exponential low. The desorption is almost complete in about 60 minutes, and about 80 percent of the deposited material comes off the ATR crystal.

Thermal desorption measurements were initiated when the vacuum desorption at room temperature was no longer apparent. In this case also, the thermal desorption is dependent on the thickness of the deposited film. For very thick films, it appears to be linear, and behavior is exponential for thin films. The linear nature of thick film desorption is much more evident in this case than for RTV-602. The desorption kinetics between the temperature range of 50°C and 85°C appears to follow a relationship as shown in Figure 3-8 of the form

$$D_T = D_o e^{-\alpha T}$$

with an activation energy α equal to $0.077°C^{-1}$.

In this case, the possibility that there is more than one activation energy of desorption is evident. It appears that there are three activation energies, one below 40°C, one between 50 to 80°C, and the third above 90°C. This is an indication that different species are probably desorbing at different temperatures. These species are in all probability different molecular weight members of the same family, indicated by the fact that the spectrum of the original material was identified.

As can be seen, most of the deposited material comes off and only about 2 percent of the material is left around 100°C.

3.3 ULTRAVIOLET RADIATION EFFECTS

The mercury-xenon lamp used was about 6 inches from the sample. At this distance, the sample had an equivalent sun factor of about 1. The effects of 2 hours of in-situ irradiation are shown in Figures 3-1 through 3-6. The absorption spectra of the two materials do not show marked differences due to irradiation. This is understandable since polymerization

only increases the chain length of the molecule without any chemical change. Occurrence of polymerization can be noticed from the increase in resolution of the siloxane band, as discussed in Section 3.1. The effect is not very pronounced since only the surface was polymerized and the material in direct contact with the ATR crystal was unpolymerized RTV-560 and 602. Longer duration of irradiation is needed to bring about structural breakdown. It is anticipated that prolonged radiation will give rise to additional bands -- one being located around 5.7 micrometers -- due to chain cleavage and fission as observed in the SL-4 contaminant spectrum (Ref. 1). Nevertheless, this duration of irradiation was sufficient to bring out the polymerization of the materials as discussed. This is also evident from the thermal desorption studies. After irradiation, as shown in Figures 3-4 and 3-6, no measurable desorption was seen for temperatures as high as 150°C.

Organic solvents did not react with the surface of the irradiated materials. The film could be removed from the ART crystal surface by making a scratch on the film and letting the solvent react with material under the top layer. The surface film left behind could not be dissolved in the usual solvents.

The polymerized surface layer was very thin, about 1,000 Å, and no spectral measurements could be made on it. The ATR crystal could have been optimized for films of this thickness and spectra obtained, but results from the thicker films were felt to be of more importance. Thickness was judged from the coloration it produced. Since the measured spectra is the result of both the silicone in contact with the ATR crystal and the polymerized film on top of it, the resolution of the silicone double band is low. It is possible that the resolution will be higher for a completely cross-linked silicone.

Thus, it is clear that 2 hours of irradiation with a high-pressure mercury lamp was sufficient to produce polymerization of the surfaces of the RTV-560 and 602 films.

3.4 IN-SITU DEPOSITION STUDY

In-situ deposition of the outgassed products from the cured materials was performed by placing the material in the contaminant dosing port and heating it (Ref. 1). Very little deposition was obtained from the small amount of material that could be put in the contaminant dosing port. The infrared spectra were similar except that they were weak because a very small amount was present on the ATR surface. RTV-560 showed less outgassing compared with RTV-602.

In-situ deposition kinetics (Figure 3-9) do not appear to be the same as vacuum-desorption kinetics. It should be noted here that the in-situ deposition studies were made by heating the cured material and monitoring the deposition, as a function of time, on the ATR of room temperature. No correlation between outgassing kinetics and deposition kinetics can be made since the heating rates of the cured materials were not known and the materials were not at a particular temperature for a known length of time.

4. CONCLUSIONS AND RECOMMENDATION

Different absorption bands of the spectra of RTV-602 and 560 can be properly identified with the various group frequencies of the chemical constituents. The methyl-silicon stretching absorption around 8 micrometers in RTV-560 is slightly shifted toward a higher wavelength as compared with RTV-602. The spectral differences between RTV-560 and 602 are the bands at 7.0, 10.3, 11.5, 12.0, and 13.5 micrometers. These bands can be used to identify these two silicones and distinguish one from the other.

Both the materials show an exponential decay of film thickness with time and temperature in vacuum. This is true for most of the middle range of time and temperature regimes studied. The activation energy of thermal decay is $0.019°C^{-1}$ for RTV-602 and $0.077°C^{-1}$ for RTV-560. The deposition kinetics are not exponential under the present study conditions.

A yellow-brown deposit was found on the ATR crystal holder facing the silicone deposited ATR crystal face after thermal desorption. This color resembled the color of the contaminant found on the SL-4 rendezvous window. This material could be easily removed with an organic solvent since, because of its location, it was not ultra-violet irradiated.

It is recommended that further experimental work be performed on silicone materials for their outgassing and desorption characteristics and chemical changes due to high irradiation doses. This will help understand the various processes through which silicones go due to long-duration ultraviolet irradiation. Irradiation studies should be performed until no further change due to irradiation is observed. This will give the ultimate effect of irradiation, which will be beneficial for space station and other long-term spacecraft missions.

It is also recommended that the contaminant dosing container be modified so that the outgassing material can be held at a particular temperature for a known length of time. This modification will allow a proper correlation between outgassing and deposition kinetics.

Answers to the following questions are necessary to reduce contaminant deposits and to find methods of cleaning the contaminants from affected surfaces:

- What is this radiation-modified contaminant?
- What was it before space irradiation?
- What is the source of the contaminant?

It is still a matter of debate whether the contaminant found on the rendezvous window of SL-4 is due to Coolenol or outgassing from silicones.

To answer the above questions, one has to proceed in the reverse order; i.e., one has to study

- What source gives what kind of contaminant
- What happens to the particular contaminant due to irradiation.

5. REFERENCES

1. T. Mookherji, "Analytical Study of Spacecraft Deposition Contamination by Internal Reflection Spectroscopy", Teledyne Brown Engineering Final Report EE-MSFC-1871, January 1975

2. T. Mookherji, "Analytical Study of Spacecraft Deposition Contamination by Internal Reflection Spectroscopy", Teledyne Brown Engineering Final Report SE-SSL-1678, December 1972

3. T. Mookherji, "Analytical Study of Spacecraft Deposition Contamination by Internal Reflection Spectroscopy", Teledyne Brown Engineering Interim Report EE-SSL-1781, December 1973

4. F. Stern, Appl. Opt. 3, p. 111, 1964

5. J. Fahrenfort, Spectrochim. Acta 17, p. 698, 1961

6. N. J. Harrick, Anal. Chem. 36, p. 118, 1964